Frequency-Dependent Electrical Conductivity of Concentrated Dispersions of Spherical Colloidal Particles

ARTICLE *in* LANGMUIR · JUNE 2008

Impact Factor: 4.46 · DOI: 10.1021/la703777g · Source: PubMed

3 AUTHORS, INCLUDING:

Bronwyn H. Bradshaw-Hajek
University of South Australia
18 PUBLICATIONS **77** CITATIONS
SEE PROFILE

Stanley J Miklavcic
University of South Australia
91 PUBLICATIONS **1,132** CITATIONS
SEE PROFILE

Frequency-Dependent Electrical Conductivity of Concentrated Dispersions of Spherical Colloidal Particles

B. H. Bradshaw-Hajek,[‡] S. J. Miklavcic,*[,‡] and L. R. White[†]

Department of Chemical Engineering, Carnegie Mellon University, Pittsburgh, Pennsylvania, School of Mathematics and Statistics, University of South Australia, Mawson Lakes, SA 5095, Australia, and Department of Science and Technology, University of Linköping, S-601 74, Norrköping, Sweden

Received December 2, 2007. In Final Form: February 3, 2008

This paper outlines the application of a self-consistent cell-model theory of electrokinetics to the problem of determining the electrical conductivity of a dense suspension of spherical colloidal particles. Numerical solutions of the standard electrokinetic equations, subject to self-consistent boundary conditions, are implemented in formulas for the electrical conductivity appropriate to the particle-averaged cell model of the suspension. Results of calculations as a function of frequency, zeta potential, volume fraction, and electrolyte composition, are presented and discussed.

I. Introduction

In a recent publication Ahualli et al.[1] presented a cell-model theory of the electrokinetics of dense suspensions of spherical particles valid for arbitrary electrolyte composition, zeta potential, ζ, and general κa, where a is the particle radius and κ is the Debye parameter of the electrolyte. Specifically, the cell model was applied to describe the dynamic mobility of a dense suspension of spherical particles in an applied electric field of volume average $\langle \mathbf{E} \rangle e^{-i\omega t}$. An ensemble averaging over all particle positions relative to a chosen particle gives rise to a symmetry-preserving, concentric spherical cell boundary of radius

$$b = a\phi^{-1/3}$$

Here, ϕ denotes the average volume fraction of the particle suspension. In ref 1 Ahualli et al. it was argued that the only reasonable conditions pertaining to the outer boundary at $r = b$ that can be implemented self-consistently are those that originate from global physical constraints. The authors thus presented a complete set of conditions applicable at the cell's inner and outer boundaries at $r = a$ and $r = b$, respectively (r being the radial coordinate from the center of the particle).[a] Some of these conditions had appeared previously in the literature [2−19] although these have not always been well motivated; some were novel.

In this paper we apply the self-consistent cell model to determine other transport properties of the suspension. Specifically, we focus attention on the complex electrical conductivity, K^*, of the suspension. This transport property is experimentally accessible through classical cell impedance measurements at megahertz frequencies. Traditionally, suspension conductance was measured in the kilohertz regime where the difficulties of subtracting the electrode impedance contribution and distinguishing the small imaginary part from the large real part of the suspension conductance rendered the experiment cumbersome and error-prone. At megahertz frequencies the electrode impedance is negligible and the real and imaginary parts become comparable. Although theories of suspension conductance for dilute suspensions are well developed,[10] the problem of interpretation in terms of the particle charge state is largely unsolved in high volume fraction systems. In terms of this theory, a suspension is considered concentrated in two senses (i) where the double layers are separate but the perturbation fields caused by the application of the electric field overlap and (ii) where the equilibrium double layers are also overlapping. Some progress has been made in the former case,[9] but a successful theory in the latter case is yet to be demonstrated. Although Ennis et al.[20,21] have developed a formalism for the interaction of two or more spheres, they acknowledge that with standard techniques it is only possible to expedite calculations for the two-sphere problem. The ability of our cell model to describe electrophoretic mobility measurements in concentrated systems[22] encourages us to present the extension of that model to the prediction of suspension conductivity. Indeed, for case (ii) systems it may be argued that a cell model should be a good approximation to the real suspension. This should be especially so in the case of suspensions

* To whom correspondence should be addressed. E-mail: stan.miklavcic@unisa.edu.au.

[†] Carnegie Mellon University.

[‡] University of South Australia and University of Linköping.

(1) Ahualli, S.; Delgado, A.; Miklavcic, S.; White, L. R. *Langmuir* **2006**, *22*, 7041.

(2) Hunter, R. J. *Colloids Surf., A* **1998**, *141*, 37.

(3) Hunter, R. J. *Foundations of Colloid Science*', 2nd Ed.; Oxford University Press: New York, 2001.

(4) O'Brien, R. W.; White, L. R. *J. Chem. Soc., Faraday Trans. II* **1978**, *74*, 1607.

(5) O'Brien, R. W.; Perrins, W. T. *J. Colloid Interface Sci.* **1984**, *99*, 20.

(6) O'Brien, R. W. *J. Colloid Interface Sci.* **1986**, *113*, 81.

(7) O'Brien, R. W. *J. Colloid Interface Sci.* **1986**, *110*, 477.

(8) O'Brien, R. W. *J. Fluid Mech.* **1988**, *190*, 71.

(9) O'Brien, R. W. *J. Fluid Mech.* **1990**, *212*, 81.

(10) Mangelsdorf, C. S.; White, L. R. *J. Chem. Soc., Faraday Trans.* **1992**, *88*, 3567.

(11) Mangelsdorf, C. S.; White, L. R. *J. Colloid Interface Sci.* **1993**, *160*, 275.

(12) Rosen, L. A.; Baygents, J. C.; Saville, D. A. *J. Chem. Phys.* **1993**, *98*, 4183.

(13) Ennis-King, J.; White, L. R. *J. Colloid Interface Sci.* **1996**, *178*, 446.

(14) Dukhin, A. S.; Shilov, V. N.; Borkovskaya, Y. B. *Langmuir* **1999**, *15*, 3452.

(15) Dukhin, A. S.; Shilov, V. N.; Ohshima, H.; Goetz, P. J. *Langmuir* **1999**, *15*, 6692.

(16) Ohshima, H. *J. Colloid Interface Sci.* **1997**, *188*, 481.

(17) Ohshima, H. *J. Colloid Interface Sci.* **1997**, *195*, 137.

(18) Carrique, F.; Arroyo, F. J.; Delgado, A. V. *J. Colloid Interface Sci.* **2001**, *243*, 351.

(19) Carrique, F.; Arroyo, F. J.; Jimenez, M. L.; Delgado, A. V. *J. Chem. Phys.* **2003**, *118*, 1945.

(20) Ennis, J.; Shugai, A. A.; Carnie, S. L. *J. Colloid Interface Sci.* **2000**, *223*, 21.

(21) Ennis, J.; Shugai, A. A.; Carnie, S. L. *J. Colloid Interface Sci.* **2000**, *223*, 37.

(22) Ahualli, S.; Delgado, A.; Miklavcic, S.; White, L. R. *J. Colloid Interface Sci.* **2007**, *309*, 342.

10.1021/la703777g CCC: $40.75
Published on Web 03/19/2008

in low dielectric fluids where the Debye screening length is typically 10−100 times larger than in aqueous suspensions.

One of the advantages of the cell model as developed by us in ref 1 and, particularly, the numerical implementation, is that it provides a very robust means of reproducing not only frequency-dependent electrokinetic properties such as dynamic mobility and the dielectric response of a dispersion of spherical particles; it also conveniently and very accurately reproduces the limiting cases of the static ($\omega = 0$) response at finite volume fraction and both the dynamic and static response at very low volume fractions. Volume fractions as low as 10^{-4} are easily accessible by the numerical routine we have implemented. Consequently, by means of the cell model one can directly access both the concentrated and dilute regimes. In order to perform the calculations, a program has been written in Fortran 90 using the COLSYS collocation package[23] to solve the appropriate system of odes. For further details on the numerical technique, see ref 1. For the interested reader, a robust and user-friendly program is available from the authors as an executable object ready to implement on standard PC or Apple hardware.

II. Global Constraints

When an applied oscillating electric field whose volume average is denoted $\langle \mathbf{E}\ (t)\rangle$ is applied to a colloidal suspension, the electrolyte ion number densities, n_j, charge density, ρ_{ch}, electrochemical potentials, μ_j, drift velocities, $\mathbf{v}_j$, ($j = 1, 2, .., N$), the hydrodynamic flow field, $\mathbf{u}$, pressure, p, and electrostatic potential, Ψ, are described by the following fundamental equations:[6,8,9]

$$\nabla^2\Psi(\mathrm{r}, t) = -\frac{1}{\epsilon_s\epsilon_0}\rho_{ch}(\mathbf{r}, t)$$

$$\rho_s\frac{\partial \mathbf{u}}{\partial t}(\mathbf{r}, t) = -\nabla p(\mathbf{r}, t) - \rho_{ch}(\mathbf{r}, t)\nabla\Psi(\mathbf{r}, t) + \eta_s\nabla^2\mathbf{u}(\mathbf{r}, t)$$

$$\nabla\cdot\mathbf{u}(\mathbf{r}, t) = 0$$

$$\mathrm{v}_j(\mathbf{r}, t) = \mathbf{u}(\mathbf{r}, t) - \frac{1}{\lambda_j}\nabla\mu_j(\mathbf{r}, t)$$

$$\frac{\partial n_j}{\partial t}(\mathbf{r}, \mathrm{t}) + \nabla\cdot[n_j(\mathbf{r}, t)\mathrm{v}_j(\mathbf{r}, t)] = 0$$

$$\mu_j(\mathbf{r}, t) = -z_j e\Phi_j(\mathbf{r}, t)$$

$$= \mu_j^\infty + z_j e\Psi(\mathbf{r}, t) + k_B T\ln[n_j(\mathbf{r}, t)]$$

with charge density

$$\rho_{ch}(\mathbf{r}, t) = \sum_{j=1}^{N} z_j e n_j(\mathbf{r}, t)$$

Here, e, ϵ_s, ϵ_0, ρ_s, η_s, z_j, λ_j, k_B, and T are the electron charge, the relative fluid dielectric permittivity, vacuum permittivity, fluid mass density, fluid viscosity, valency and ionic drag coefficients of the jth ion type, Boltzmann constant, and temperature, respectively. The ion densities, n_j^∞, are those of this reservoir. The drag coefficient, λ_j, is related to the ionic limiting conductance, Λ_j^∞, by

$$\lambda_j = \frac{N_A e^2|z_j|}{\Lambda_j^\infty}$$

where N_A is Avogadro's number. The electrochemical potential functions $\Phi_j(\mathbf{r}, t)$ represent the deviations of the local ion densities from their (equilibrium) Poisson−Boltzmann expressions in terms of the local electrostatic potential $\Psi(\mathbf{r}, t)$. For a more detailed explanation of these equations see ref 1. The Debye parameter is given by

$$\kappa^2 = \sum_{j=1}^{N}\frac{e^2 z_j^2 n_j^\infty}{\epsilon_s\epsilon_0 k_B T}$$

Under the influence of the oscillating electric field, the field variables deviate from their equilibrium values.[6,8,9] The deviation is supposed sufficiently weak that only the first-order perturbation correction

$$\Xi(\mathbf{r}, t) = \Xi^{(0)}(\mathbf{r}) + \Xi^{(1)}(\mathbf{r}, t) + O(\langle\mathbf{E}(t)\rangle^2) \quad (1)$$

is needed. Here Ξ represents any of the field variables, Φ_j,Ψ, $\mathbf{u}$, ρ_{ch}, μ_j, n_j, and p, with $\Xi^{(0)}$ representing the respective field-independent equilibrium contributions and $\Xi^{(1)}$ the contributions that are linearly dependent on the average external field, $\langle\mathbf{E}(t)\rangle$. For an oscillatory applied field,

$$\langle\mathbf{E}(t)\rangle = \langle\mathbf{E}\rangle e^{-i\omega t} \quad (2)$$

the first-order contributions to the perturbed fields can be expressed as a linear response,

$$\Xi^{(1)}(\mathbf{r}, t) = \Xi^{(1)}(\mathbf{r})e^{-i\omega t} \quad (3)$$

where $\Xi^{(1)}(\mathbf{r})$ is linearly proportional to $\langle\mathbf{E}\rangle$. For brevity, we will omit the $e^{-i\omega t}$ factor in all first-order field quantities in what follows.

As discussed in our previous paper on the cell model in electrokinetics,[1] since there are no useful boundary conditions pertaining to the instantaneous Wigner−Seitz cell surrounding each particle that can be ensemble-averaged to yield directly conditions on the cell boundary, the outer boundary conditions on the field quantities must be obtained from the global constraints on the suspension. The most obvious of these global constraints is the definition

$$\langle\mathbf{E}\rangle = \frac{1}{V}\int_V \mathbf{E}\ \mathrm{d}V = \frac{1}{V}\int_V(-\nabla\Psi)\ \mathrm{d}V \quad (4)$$

where V is a statistically significant sample volume around any given point in the suspension, $\langle\mathbf{E}\rangle$ is the volume-averaged electric field at that point, and Ψ is the local electrostatic potential in the neighborhood of the point. Thus, in the cell model we impose the constraint

$$\langle\mathbf{E}\rangle = \frac{1}{V_{cell}}\int_{V_{cell}}(-\nabla\Psi)\ \mathrm{d}V \quad (5)$$

Other (less obvious) global constraints are

$$\langle\nabla n_j\rangle = 0 \quad (j = 1,...N) \quad (6)$$

which expresses the necessity of suppressing diffusiophoresis in our calculation of electrophoretic motion of the particles, and

$$\langle\nabla p\rangle = 0 \quad (7)$$

(23) Ascher, U.; Christiansen, J.; Russell, R. D. COLSYS, Netlib, http://www.netlib.org.

which expresses the necessity of suppressing pressure-driven flows. When these constraints are applied to the cell, as in outer boundary conditions on the relevant quantities result, as discussed in our previous paper[1] and as listed below (eqs 32−34).

In addition to these constraints defining the electrophoresis problem, we invoke the force balance on a typical particle

$$-i\omega V_p \rho_p \mu \langle \mathbf{E} \rangle = \int_{A_p} \sigma \cdot \hat{\mathbf{n}} \, dS = \int_A \sigma \cdot \hat{\mathbf{n}} \, dS + i\omega \rho_s \int_{V_s} \mathbf{u}(\mathbf{r}) \, dV \quad (8)$$

where V_p is the particle volume, A_p is the surface of the particle, $\sigma(\mathbf{r})$ is the total stress tensor in the fluid, A is the surface of any closed bounding surface in the fluid surrounding the particle, and V_s is the enclosed fluid volume. The mass densities of the medium and particles are ρ_s and ρ_p, respectively. In the cell model, A becomes the outer boundary surface at $r = b$ and $V_s = V_{cell} - V_p$ is the fluid volume in the cell. Due to the electroneutrality of the cell and the spatial uniformity of $\langle \mathbf{E} \rangle$, only the hydrodynamic stress contributes to the integral over A in ref 8. This results in an outer boundary condition on the flow field $\mathbf{u}(\mathbf{r})$ in the cell model (see eq 36 below).

We require an additional constraint on the flow field to close the problem. As shown by O'Brien,[9] the volume-averaged momentum balance for the suspension reduces to

$$-i\rho\omega\bar{\mathbf{u}} = -\nabla\langle p \rangle \quad (9)$$

where $\bar{\mathbf{u}}$ is the mass-averaged velocity

$$\bar{\mathbf{u}} = \frac{1}{\rho V} \int_V \rho(\mathbf{r}) \mathbf{u}(\mathbf{r}) \, dV \quad (10)$$

$\rho(\mathbf{r})$ is the local mass density

$$\rho(\mathbf{r}) = \begin{cases} \rho_p & r < a \\ \rho_s & a < r < b \end{cases}$$

and

$$\rho = \rho_s + \phi(\rho_p - \rho_s) = \rho_s + \phi\Delta\rho \quad (11)$$

is the volume-averaged suspension density. Equation 9 is correct to terms of order a/λ, where a is the particle size and λ is the wavelength of sound in the suspension. Together with eq 7, eq 9 implies

$$\bar{\mathbf{u}} = 0 \quad (12)$$

It should be noted that, in our previous paper,[1] we invoked the constraint

$$\langle \mathbf{u} \rangle = 0 \quad (13)$$

consistent with Kuwabara's second condition on the flow field.[24] Consequently, our development of the electrophoresis problem in that paper was *incorrect* although, numerically, the results displayed there would be only slightly altered by this correction. We amend that development in the next section. The two ensemble-averaged velocities are related by[9]

$$\rho\bar{\mathbf{u}} = \rho_s\langle \mathbf{u} \rangle + \phi\Delta\rho\mu\langle \mathbf{E} \rangle \quad (14)$$

which may be simply derived from the definition eq 10 by writing

$$\rho(\mathbf{r}) = \rho_s + \phi(\rho(\mathbf{r}) - \rho_s) \quad (15)$$

In the small volume fraction limit the two approaches are indistinguishable but at higher volume fractions and, as we shall show below, at high frequencies they may differ significantly.

III. Cell Model of Colloidal Electrokinetics

By inserting expansion into the field equations[1] we obtain a hierarchy of equations which must be solved to obtain the electrokinetic properties of interest.

The zeroth-order contributions satisfy the field equations

$$\begin{cases} n_j^{(0)}(r) = n_j^{\infty} \exp(-z_j e \Psi^{(0)}(r)/k_B T) \\ \rho_{ch}^{(0)}(r) = \sum_{j=1}^{N} z_j e n_j^{(0)}(r) \end{cases} \quad (16)$$

$$p^{(0)}(r) = p_{amb} + \sum_{j=1}^{N} (n_j^{(0)}(r) - n_j^{\infty}) k_B T \quad (17)$$

$$\mu_j^{(0)}(r) = -z_j e \Phi_j^{(0)}(r) = \mu_j^{\infty} + k_B T \ln n_j^{\infty} \quad (18)$$

$$\frac{1}{r^2}\frac{d}{dr}\left(r^2 \frac{d\Psi^{(0)}}{dr}(r)\right) = \begin{cases} 0 & r < a \\ -\dfrac{\rho_{ch}^{(0)}(r)}{\epsilon_s \epsilon_0} & a < r < b \end{cases} \quad (19)$$

In eq 17 p_{amb} is the ambient pressure in the reservoir that is in equilibrium with the suspension. These equations are solved subject to the following conditions.

At the slipping plane at each particle surface, $r = a$

$$\Psi^{(0)}|_{r=a} = \zeta \quad (20)$$

while at the outer extreme of the cell, global electro-neutrality forces

$$\frac{d\Psi^{(0)}}{dr}|_{r=b} = 0 \quad (21)$$

At first order, the dipolar symmetry suggests the independent variable separation

$$\Xi^{(1)}(\mathbf{r}) = \xi(r) \langle \mathbf{E} \rangle \cdot \hat{\mathbf{r}} \quad (22)$$

where $\Xi^{(1)}(\mathbf{r})$ represents any of the first-order perturbed quantities $\Psi^{(1)}(\mathbf{r})$, $\Phi_j^{(1)}(\mathbf{r})$ and $p^{(1)}(\mathbf{r})$, and $\xi(r)$ represents corresponding coefficient functions, $\psi(r)$, $\phi_j(r)$, and $P(r)$. Symmetry also ensures the fluid velocity form (in the reference frame of the central particle)

$$\mathbf{u}^{(1)}(\mathbf{r}) = (u_r, u_\theta, u_\phi) = \mu(\omega)\langle \mathbf{E} \rangle - \left(\frac{2h(r)}{r}\langle \mathbf{E} \rangle \cdot \hat{\mathbf{r}}, \frac{1}{r}\frac{\partial(rh(r))}{\partial r}[\langle \mathbf{E} \rangle - \langle \mathbf{E} \rangle \cdot \hat{\mathbf{r}}\hat{\mathbf{r}}] \cdot \hat{\boldsymbol{\theta}}, 0\right) \quad (23)$$

where $\mu(\omega)$ is the electrophoretic mobility and $h(r)$ is an intermediate function. Thus, the first-order problem involves the following coupled set of complex ordinary differential equations for the functions ψ, ϕ_j, and h[6]

$$L\psi(r) = \frac{e^2}{\epsilon_s \epsilon_0 k_B T} \sum_{j=1}^{N} z_j^2 n_j^0(r)[\phi_j(r) + \psi(r)] \quad (24)$$

(24) Kuwabara, S. *J. Phys. Soc. Jpn.* **1959**, *47*, 527.

$$L\phi_j(r) + \gamma_j^2[\phi_j(r) + \psi(r)] = \frac{e}{k_B T}\frac{d\Psi^{(0)}}{dr}(r)\left(z_j\frac{d\phi_j(r)}{dr} - \frac{2\lambda_j}{e}\frac{h(r)}{r}\right) \quad (25)$$

and

$$L(L+\gamma^2)h(r) = -\frac{e^2}{\eta_s k_B T}\frac{1}{r}\frac{d\Psi^{(0)}}{dr}\sum_{j=1}^{N} z_j^2 n_j^0(r)\phi_j(r) \quad (26)$$

where we have introduced the constants

$$\gamma = \frac{(1+i)}{\sqrt{2}}\sqrt{\frac{\omega\rho_s}{\eta_s}}, \quad \gamma_j = \frac{(1+i)}{\sqrt{2}}\sqrt{\frac{\omega\lambda_j}{k_B T}} \quad (27)$$

and the second-order differential operator

$$L = \frac{d^2}{dr^2} + \frac{2}{r}\frac{d}{dr} - \frac{2}{r^2} \quad (28)$$

The corresponding boundary conditions are, at $r = a$

$$h(a) = \frac{dh}{dr}|_{r=a} = 0 \quad (29)$$

$$\frac{d\phi_j}{dr}|_{r=a} = 0 \quad (30)$$

$$\frac{d\psi}{dr}|_{r=a} - \frac{\epsilon_p}{\epsilon_s a}\psi(a) = 0 \quad (31)$$

At $r = b$, global constraint eq 5 yields

$$\psi(b) = -b \quad (32)$$

eq 6 yields

$$\phi_j(b) = b \quad (33)$$

and eq 7 yields

$$\frac{d}{dr}[r(L+\gamma^2)h]|_{r=b} - \mu\gamma^2 b - \frac{\rho_{ch}^{(0)}(b)b}{\eta_s} = 0 \quad (34)$$

as derived in ref 1. Global constraint eq 12 yields

$$\mu = \frac{2h(b)}{b}\left[1 + \phi\frac{\Delta\rho}{\rho_s}\right]^{-1} \quad (35)$$

Note that this differs from the result derived in ref 1 by the inclusion of the $(1 + \phi\Delta\rho/\rho_s)$ factor. The particle force balance condition (eq 8) then becomes

$$Lh|_{r=b} = \frac{\gamma^2 b}{2}\left[\mu\left(1 + \phi\frac{\Delta\rho}{\rho_s}\right) - \frac{2h(b)}{b}\right] \quad (36)$$

and, with the aid of eq 35, this becomes

$$Lh|_{r=b} = 0 \quad (37)$$

Interestingly enough, this is just the first Kuwabara condition,[24] $(\nabla \times \mathbf{u})|_{r=b} = 0$, made explicit for our cell model. Finally, substituting eqs 35 and 37 into eq 34 yields

$$\frac{d}{dr}[(L+\gamma^2)h]|_{r=b} = \frac{\gamma^2 h(b)}{b}\frac{\left(1 - \phi\frac{\Delta\rho}{\rho_s}\right)}{\left(1 + \phi\frac{\Delta\rho}{\rho_s}\right)} + \frac{\rho_{ch}^{(0)}(b)}{\eta_s} \quad (38)$$

IV. Dielectric Response

We begin the derivation of conductivity by first defining the local current,

$$\mathbf{i}(r) = \sum_{j=1}^{N} n_j^0(r) z_j e v_j(r) + i\omega\epsilon(r)\nabla\psi(r) \quad (39)$$

which, using the cell model equations, can be rewritten as

$$\mathbf{i}(r) = \rho_{ch}^{(0)}(r)\,\mathbf{u}\,(r) - \sum_{j=1}^{N}\frac{z_j e n_j^0(r)}{\lambda_j}\nabla\mu_j^{(1)}(r) + i\omega\epsilon(r)\nabla\psi(r) \quad (40)$$

where

$$\epsilon(r) = \begin{cases}\epsilon_p\epsilon_0 & r < a \\ \epsilon_s\epsilon_0 & a < r < b\end{cases} \quad (41)$$

Now, applying Gauss' integral theorem to the volume average definition we have

$$\langle\mathbf{i}\rangle = \frac{1}{V_{cell}}\int_{V_{cell}} dV\nabla\cdot(\mathbf{ri}) = \frac{1}{V_{cell}}\int_{(r=b)} (\mathbf{ri})\cdot\hat{\mathbf{r}}\, dS \quad (42)$$

where, upon inserting the expression for $\mathbf{i}(r)$, we find

$$\langle\mathbf{i}\rangle = \frac{3}{4\pi}\int_{(r=b)}\left(\rho_{ch}^{(0)}(r)\,\mathbf{u}\,(r)\cdot\hat{\mathbf{r}} - \sum_{j=1}^{N}\frac{z_j e n_j^0(r)}{\lambda_j}\nabla\mu_j^{(1)}(r)\cdot\hat{\mathbf{r}} + i\omega\epsilon\,(r)\,\nabla\psi\,(r)\cdot\hat{\mathbf{r}}\right)|_{r=b}\hat{\mathbf{r}}\, dS$$

However, from eq 23 and the boundary conditions applicable at the cell boundary, $r = b$, we have that

$$(\mathbf{u}\,(r)\cdot\hat{\mathbf{r}})|_{r=b} = \left(\mu - \frac{2h(b)}{b}\right)\langle\mathbf{E}\rangle\cdot\hat{\mathbf{r}}$$

$$(\nabla\mu_j^{(1)}(r)\cdot\hat{\mathbf{r}})|_{r=b} = -z_j e\nabla\Phi_j\cdot\hat{\mathbf{r}}$$

$$= -z_j e\left(\frac{d\phi_j}{dr}\right)|_{r=b}\langle\mathbf{E}\rangle\cdot\hat{\mathbf{r}}$$

and

$$(\nabla\psi(r)\cdot\hat{\mathbf{r}})|_{r=b} = \left(\frac{d\psi}{dr}\right)|_{r=b}\langle\mathbf{E}\rangle\cdot\hat{\mathbf{r}}$$

Thus,

$$\langle\mathbf{i}\rangle = \frac{3}{4\pi}\left(\rho_{ch}^{(0)}(b)\left(\mu - \frac{2h(b)}{b}\right) + \sum_{j=1}^{N}\frac{z_j^2 e^2 n_j^0(b)}{\lambda_j}\frac{d\phi_j}{dr}(b) + i\omega\epsilon_s\epsilon_0\frac{d\psi}{dr}(b)\right)\times\langle\mathbf{E}\rangle\cdot\int_{(r=b)}\hat{\mathbf{r}}\hat{\mathbf{r}}\, dS \quad (43)$$

with the remaining integral contributing a factor, $4\pi/3\overleftrightarrow{I}$, where $\overleftrightarrow{I}$ is the unit second-order tensor. Equating eq (43) to the product of conductivity and mean field,

$$\langle \mathbf{i} \rangle = K^* \langle \mathbf{E} \rangle \tag{44}$$

and using eq 35 we arrive at a complex conductivity given by

$$K^* = -\rho_{ch}^{(0)}(b)\mu\frac{\Delta\rho}{\rho_s}\phi + \sum_{j=1}^{N}\frac{z_j^2 e^2 n_j^0(b)}{\lambda_j}\frac{d\phi_j}{dr}(b) + i\omega\epsilon_s\epsilon_0\frac{d\psi}{dr}(b) \tag{45}$$

This conductivity expression contains a contribution from the charged particle dispersion and associated electrical double layers as well as the contribution from the bulk electrolyte,

$$K_{sol}^* = \sum_{j=1}^{N}\frac{z_j^2 e^2 n_j^\infty}{\lambda_j} - i\omega\epsilon_s\epsilon_0 \tag{46}$$

However, it is the deviation of the conductivity from this bulk value that is of predominant interest. This deviation can be written in two ways of interest to experimentalists. The first form

$$K^* = K_{sol}^* + \Delta K^* \tag{47}$$

explicitly focuses attention on the deviation from the bulk conductivity. The second form introduces the so-called dipole strength, C,

$$K^* = K_{sol}^*\left(\frac{1+2\phi C}{1-\phi C}\right) \tag{48}$$

In the past, this second form has often been approximated by the low volume fraction expression, $K^* = K_{sol}^*(1 + 3\phi C_{approx})$, commonly appearing in theoretical works such as refs 5, 6, and 25. From eq 45 we have explicitly

$$\Delta K^* = \sum_{j=1}^{N}\frac{z_j^2 e^2 n_j^\infty}{\lambda_j}\left[\exp(-z_j e\Psi^0(b))\frac{d\phi_j}{dr}(b) - 1\right] - \rho_{ch}^{(0)}(b)\mu\frac{\Delta\rho}{\rho_s}\phi + i\omega\epsilon_s\epsilon_0\left[\frac{d\psi}{dr}(b) + 1\right] \tag{49}$$

which vanishes in the absence of an electrical field, as well as in the absence of particles. From eq (48) we have that

$$C = \frac{1}{\phi}\frac{\Delta K^*/K_{sol}^*}{3 + \Delta K^*/K_{sol}^*} \tag{50}$$

from which we deduce the low volume fraction approximation, $C_{approx} = \Delta K^*/K_{sol}^*/(3\phi)$.

V. Numerical Results and Discussion

In this section we present the results of our conductivity calculations in two forms: through the complex conductivity increment, ΔK^*, and the effective dipole coefficient, C. As the physical properties of ΔK^* are easiest to access, we begin our discussion with this quantity. Second, we are interested in reviewing the dependencies of the effective dipole coefficient on certain physical quantities, in particular volume fraction, to determine the range of applicability of the Maxwell−Wagner formula (eq 48).

Table 1. Electric and Fluid Dynamic Data Used to Generate All Graphs in This Paper

relative permittivity of medium	$\epsilon_s = 78.54$
relative permittivity of particle	$\epsilon_p = 2.0$
medium viscositys	$\eta_0 = 0.8904$ cP
medium density	$\rho_s = 0.997$g cm^{-3}
particle density	$\rho_p = 1.05$g cm^{-3}
temperature	$T = 298.16$ K
limiting conductance of cation (g equiv)$^{-1}$	$\Lambda_+^\infty = 73.5$ cm^2 Ω^{-1}
limiting conductance of anion (g equiv)$^{-1}$	$\Lambda_-^\infty = 76.35$ cm^2 Ω^{-1}

In this paper we study a similar, though slightly larger, space of electrical double layer parameters—ζ potential and κa—to that studied in ref 25. Having said this, we recognize that the full extent of parameter space is unwieldy to explore in a single report. For this reason we focus attention mainly on the volume fraction dependence of ΔK^* and C for representative values of the above double layer parameters and as functions of frequency in order to compare directly with those earlier results. We are particularly interested in identifying any volume fraction dependence of the dipole coefficient, C. We further remark that in a previous publication[1] we presented a comparison between frequency-dependent dynamic mobilities as predicted by the present cell model and those predicted by other cell models. Since we anticipate that similar conclusions would be drawn from an analogous comparison of conductivities, we forego this comparison here.

A. Complex Conductivity Increment. Figures 1−3, 4−6, 7−9, and 10−12 show the frequency response of the complex conductivity increment at increasing volume fractions for three

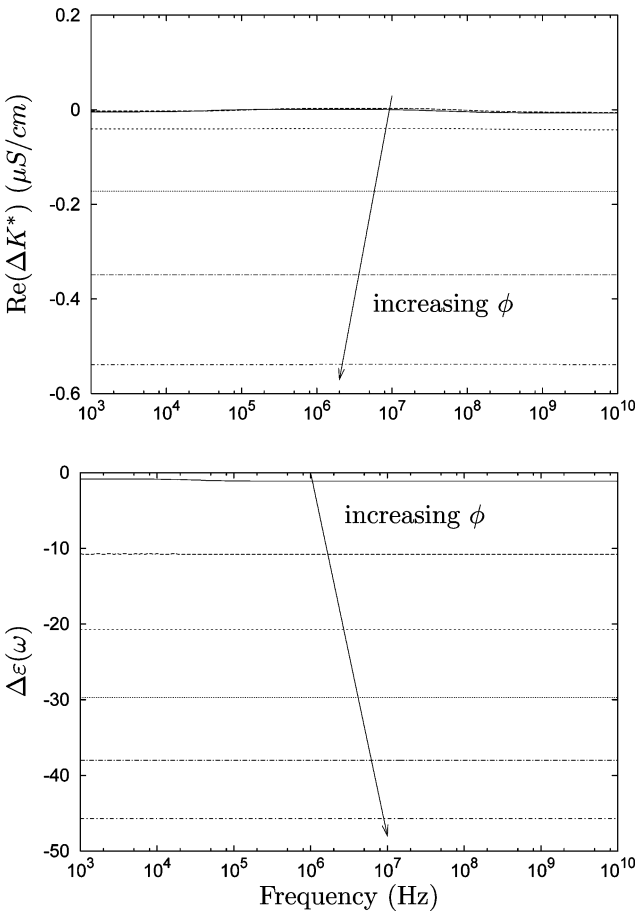

Figure 1. Frequency response of the (a) real part of the conductivity increment, Re($\Delta K^*(\omega)$) and (b) dielectric permittivity increment for $\phi \in \{10^{-2}, 0.1, 0.2, 0.3, 0.4, 0.5\}$. Reduced ζ potential is $e\zeta/k_BT = 1$ and $\kappa a = 1$.

(25) Mangelsdorf, C. S.; White, L. R. *J. Chem. Soc., Faraday Trans.* **1997**, *93*, 3145.
(26) Carrique, F.; Arroyo, F. J.; Delgado, A. V. *J. Colloid Interface Sci.* **2002**, *252*, 126.

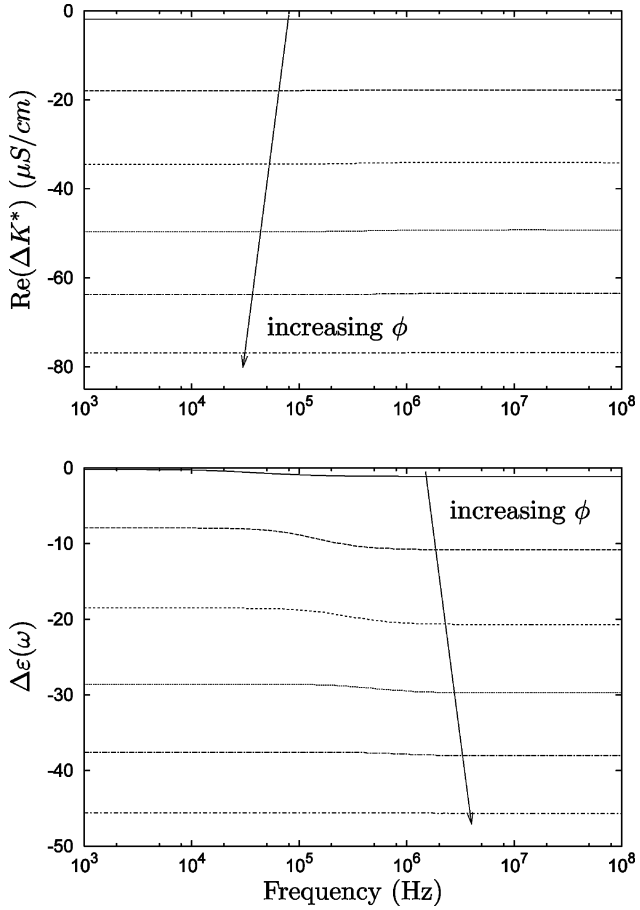

Figure 2. As in Figure 1 ($e\zeta/k_BT = 1$) except $\kappa a = 10$.

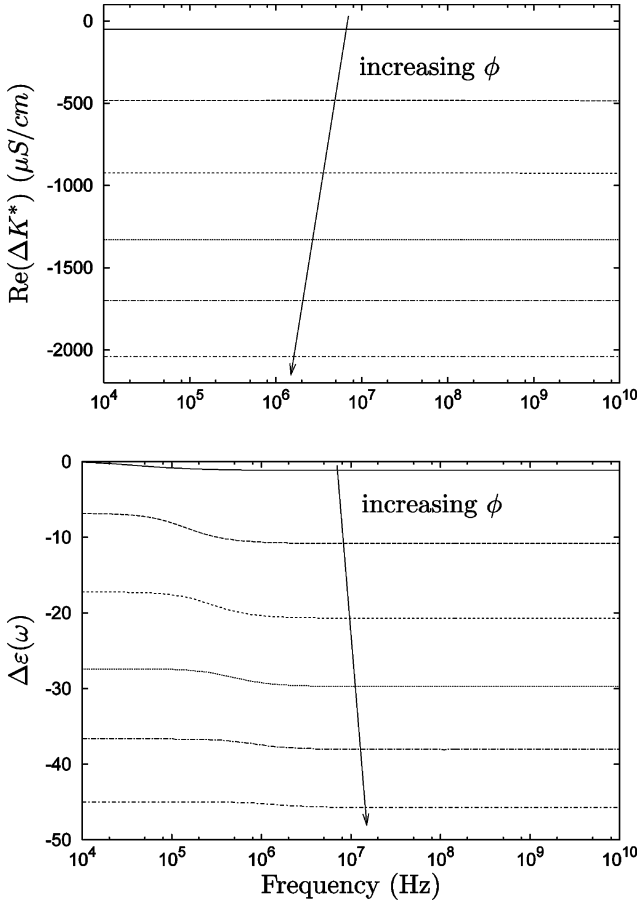

Figure 3. As in Figure 1 ($e\zeta/k_BT = 1$) except $\kappa a = 50$.

electrolyte concentrations and for reduced ζ potentials of $e\zeta/k_BT = 1,4,7$, and 10, respectively. The real part of the conductivity increment is shown in parts a. Parts b show the dielectric permittivity increment, given by

$$\Delta\epsilon(\omega) = \frac{-\mathrm{Im}(\Delta K^*(\omega))}{\omega\epsilon_0}$$

Both the real part of the complex conductivity increment and the dielectric permittivity are experimentally measurable quantities. We begin our discussion with the *real part* of the complex conductivity increment.

With the exception of those with the lowest ζ potential, all systems studied show a peak in the conductivity increment at a threshold frequency between 1 and 1000 MHz. Below this threshold frequency, the conductivity increment increases with frequency, while above this threshold frequency, the conductivity increment decreases. The transition can be explained by considering the influence of the double layer surrounding each particle.[25] As the oscillating field changes direction, the diffuse double layer must move from one side of the particle to the other. Once the oscillation period of the field becomes shorter than the time it takes for the ion cloud to move this distance, the double layer can no longer follow the oscillations of the field. At this point, the conductivity increment decreases as frequency increases. As κa increases (i.e., for thinner double layers), the threshold frequency shifts to higher frequencies. This shift can be accounted for by considering the size of the double layer. For large κa systems, the double layer is thin and the amount of time required for the ion cloud to move from one side of the particle to the other is reduced. Therefore, the moving ions can follow the applied field to higher frequencies.

We have confirmed the finding[27] that increasing the ζ potential increases the conductivity (for example, follow the sequence of Figures 2, 5, 8, and 11). For fixed κa, this is because a greater number of mobile ions are drawn into the double layer at higher ζ potentials.

For fixed large ζ potentials, increasing κa also increases the conductivity since there are more ions in the double layer, as well as in the bulk.

For fixed small ζ potentials, increasing the volume fraction decreases the conductivity so that the ΔK^* becomes negative. This is a consequence of the presence of the low dielectric solid particles (i.e., their low dielectric permittivity and the fact that they hinder ion movement). At larger ζ potentials the number of mobile ions around the charged particles is larger, thus compensating for the presence of the low dielectric particles, so that increasing the volume fraction increases the conductivity.

We now discuss the behavior of the dielectric permittivity increment (i.e., the imaginary part of ΔK^*).

At high frequencies, the dielectric response increment is negative. This is a consequence of the mechanism, described above, responsible for the peak and subsequent decrease in the conductivity increment above the threshold frequency.[27] For very high frequencies, the period of field oscillation is shorter than the period of the ion cloud oscillation around the particle. Once the frequency is high enough, the dielectric permittivity increment approaches a negative value corresponding to the $\zeta = 0$ case and is independent of κa. The dielectric permittivity increment is negative for the $\zeta = 0$ case because some of the high dielectric bulk electrolyte solution has been replaced by low dielectric particles.

(27) DeLacey, E. H. B.; White, L. R. *J. Chem. Soc., Faraday Trans.* **1981**, 2, *77*, 2007.

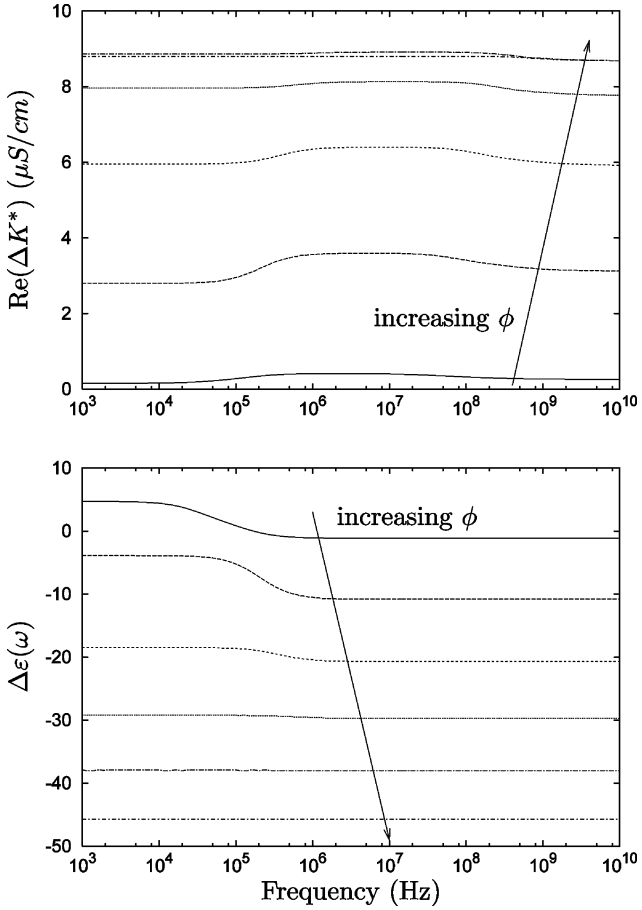

Figure 4. As in Figure 1 except $e\zeta/k_BT = 4$ ($\kappa a = 1$).

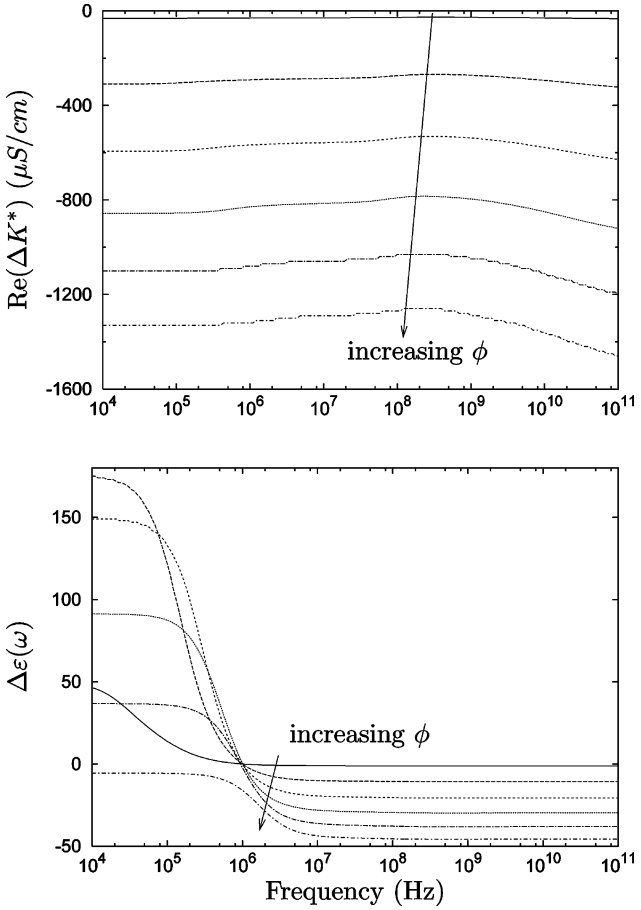

Figure 6. As in Figure 4 ($e\zeta/k_BT = 4$) except $\kappa a = 50$.

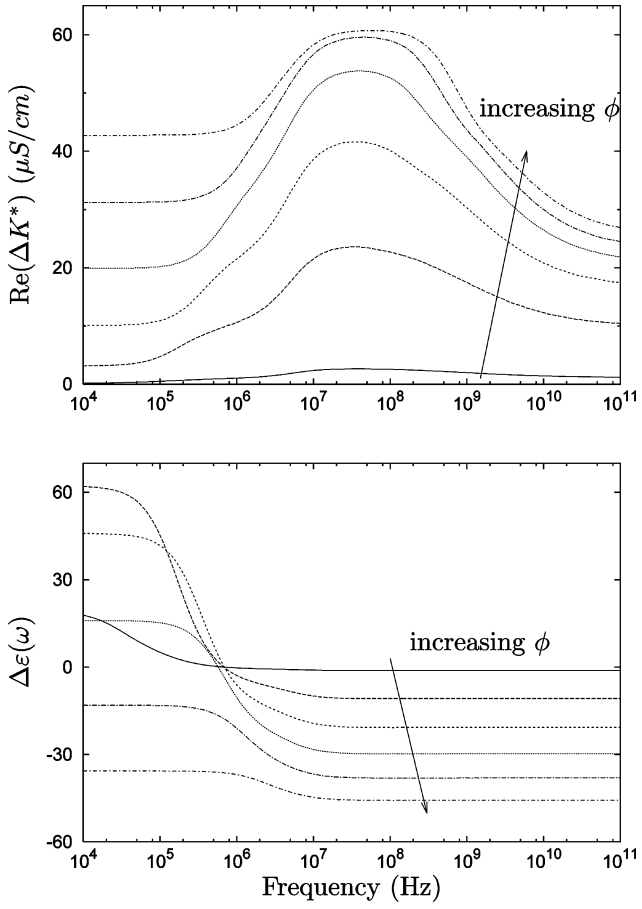

Figure 5. As in Figure 4 ($e\zeta/k_BT = 4$) except $\kappa a = 10$.

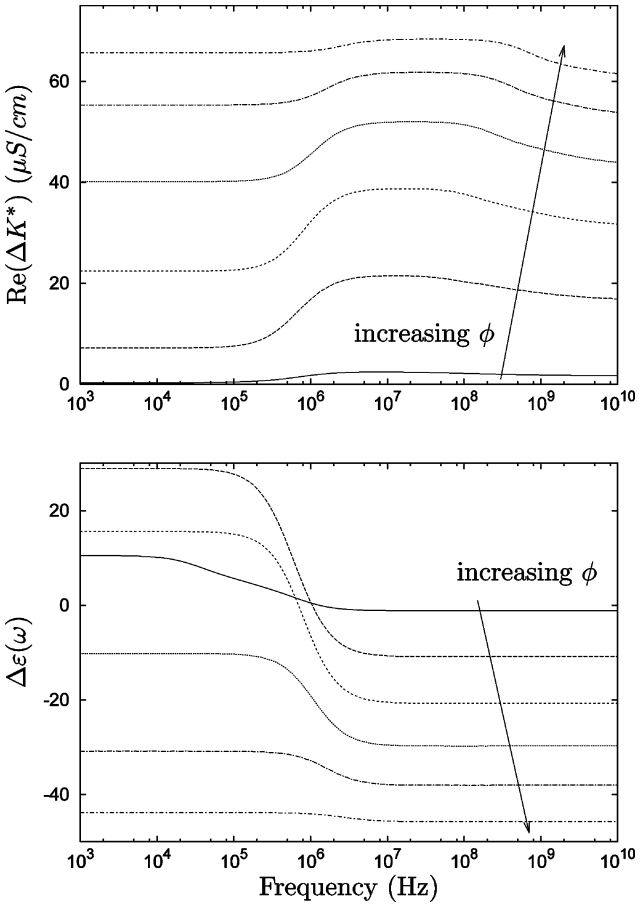

Figure 7. As in Figure 1 except $e\zeta/k_BT = 7$ ($\kappa a = 1$).

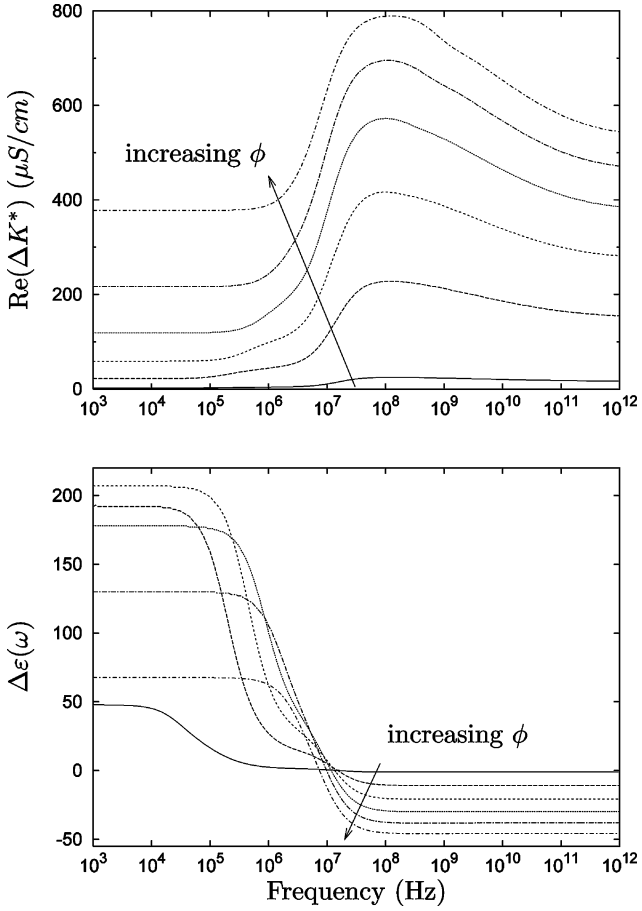

Figure 8. As in Figure 7 ($e\zeta/k_BT = 7$) except $\kappa a = 10$.

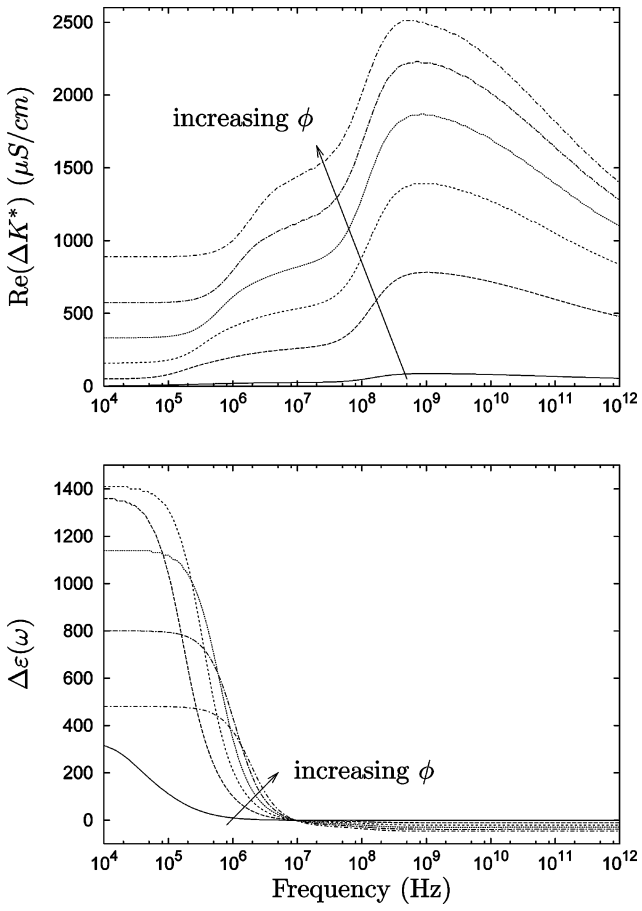

Figure 9. As in Figure 7 ($e\zeta/k_BT = 7$) except $\kappa a = 50$.

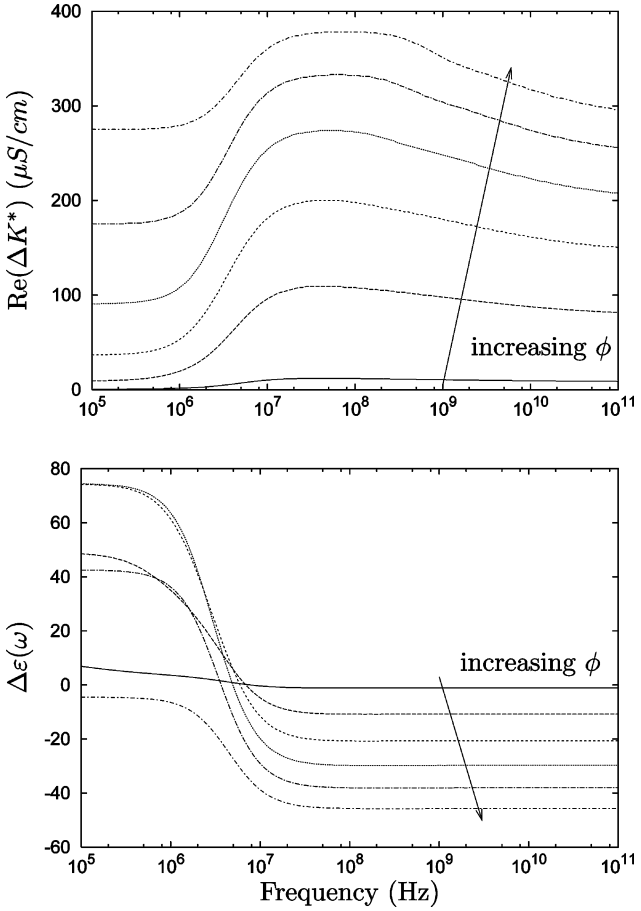

Figure 10. As in Figure 1 except $e\zeta/k_BT = 10$ ($\kappa a = 1$).

At low frequencies, variation of the permittivity with volume fraction is more complicated. At low ζ potentials, the effect of the low dielectric particles is prominant, so that increasing the volume fraction decreases the permittivity increment. At high ζ potentials, increasing the volume fraction increases the number of mobile ions in the double layers around particles, thus increasing the permittivity increment. For intermediate values of the ζ potential, there is a competition between these two effects, so that the permittivity increment is not monotonic in volume fraction.

As the ζ potential increases, the permittivity increment increases because there are more ions in the double layer. Similarly, the permittivity increment increases as κa increases. This is because, for a fixed ζ potential and particle size, there are more ions in the double layer.

B. Maxwell−Wagner Dipole Coefficient. Finally, we examine the Maxwell−Wagner expression for the dipole coefficient. Some past works (for example, see refs 5, 6, 25) feature the frequency dependence of the dipole coefficient, C. The coefficient usually appears as a proportionality constant in a first-order approximation to the solution conductivity, $3K^*_{sol}C_{approx}\phi$. The explicit linear dependence on ϕ in this first-order perturbation implies that the coefficient is independent of ϕ. Generally, the expression is limited to low volume fractions; beyond this range of validity, deviations from linear ϕ-dependence are manifested in a ϕ-dependent C. Similarly, the Maxwell−Wagner expression (eq 48) approximately describes the change in solution conductivity due to a finite particle concentration. This expression, going beyond linear response, is arguably valid to larger volume fractions and assumes the coefficient is again ϕ independent. In the very dilute limit, the two expressions become identical to first order.

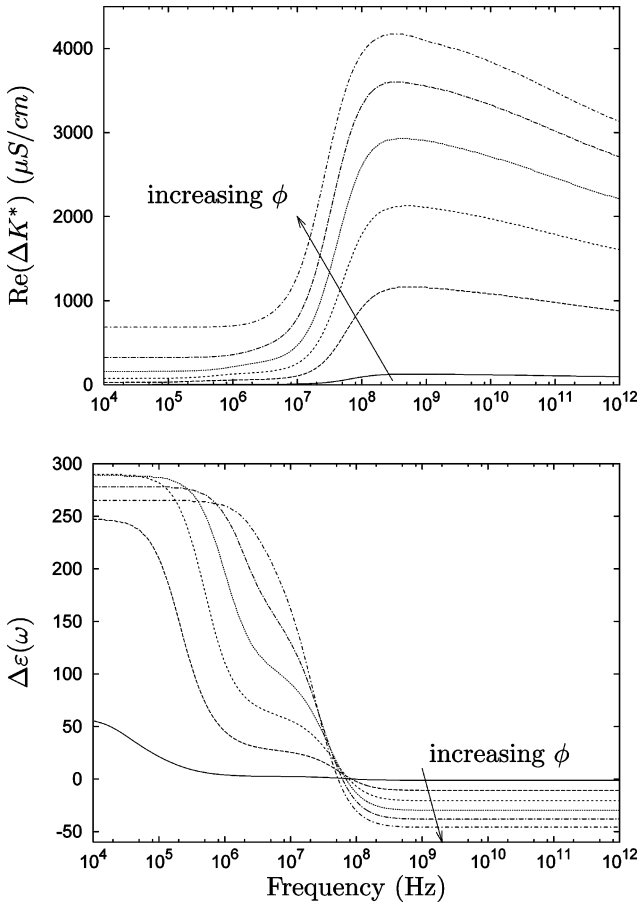

Figure 11. As in Figure 10 ($e\zeta/k_BT = 10$) except $\kappa a = 10$.

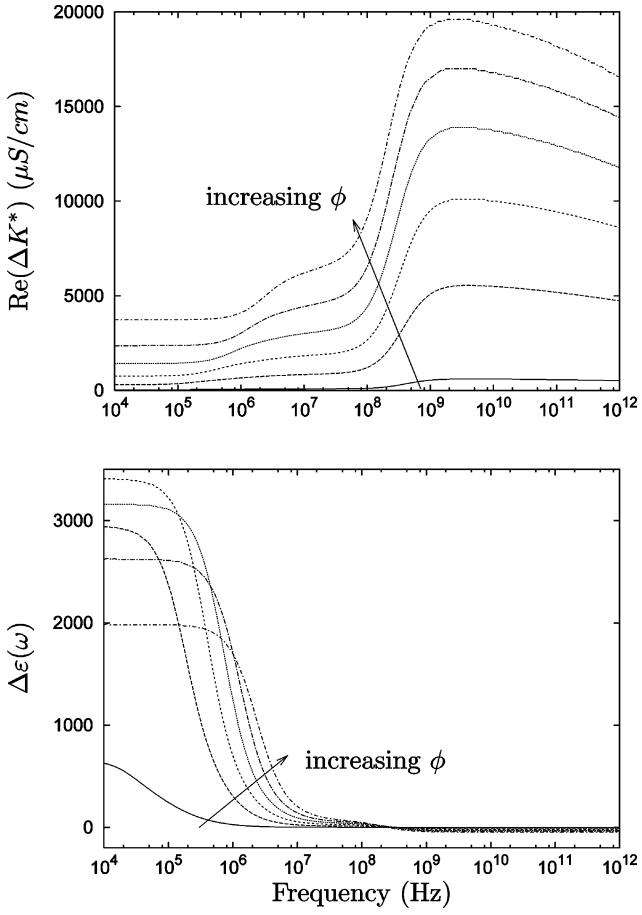

Figure 12. As in Figure 10 ($e\zeta/k_BT = 10$) except $\kappa a = 50$.

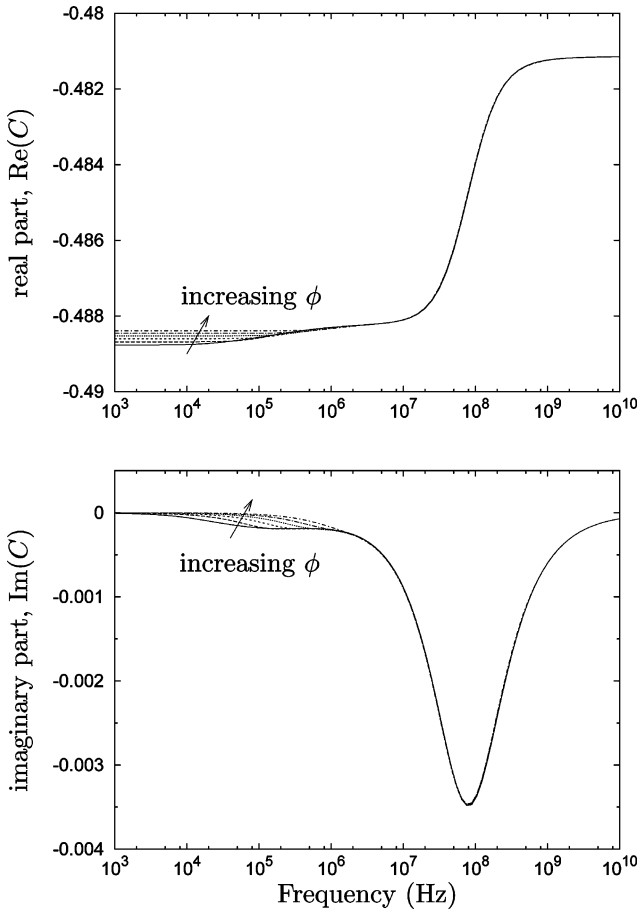

Figure 13. Frequency response of the (a) real and (b) imaginary parts of the Maxwell−Wagner dipole coefficient, C for $\phi \in \{10^{-2}, 0.1, 0.2, 0.3, 0.4, 0.5\}$. Electrolyte concentration is 2.31×10^{-2} M, $\kappa a = 50$, and reduced ζ potential is $e\zeta/k_BT = 1$.

Figures 13−16 show the frequency response of the Maxwell−Wagner dipole coefficient, C, for thin double layers, $\kappa a = 50$ at various ζ potentials. The real and imaginary parts are shown in parts a and b, respectively.

In a comparison of $\Delta K^*/K^*_{sol}$ with results of DeLacey and White[27] and Mangelsdorf and White,[25] our low volume fraction results ($\phi \leq 10^{-2}$, not shown) for the frequency dependence of C agree to high accuracy. Thus, the present cell-model methodology proves to be a practical and expedient alternative to the asymptotic methods of White, et al.[25,27] for determining the conductivities of very dilute dispersions. At the same time, the model also reproduces the static limit of the conductivity at finite volume fractions. We have previously made mention of a similar advantage in the context of determining the dynamic mobility.[1] We note in passing that in ref 25 the authors have neglected to explicitly indicate that their numerical dipole coefficient results include a normalizing factor of a^3. This is not apparent from the definition given in their eq 9.

For thin double layers, $\kappa a = 50$, the dipole coefficient is independent of volume fraction when $\phi \leq 10^{-2}$ and largely independent of volume fraction when $\phi \geq 10^{-1}$. However, for high volume fractions the dependence on ϕ increases as ζ potential increases. To see this, the reader can follow the sequence in Figures 13−16. Presumably, when the double layers are sufficiently thin and surface potential low, so that little interaction arises between particles, a first-order conductivity response to volume fraction increases is adequately encompassed by eq 48. As particle interactions increase with ζ potential, a more significant volume fraction dependence of C is noted.

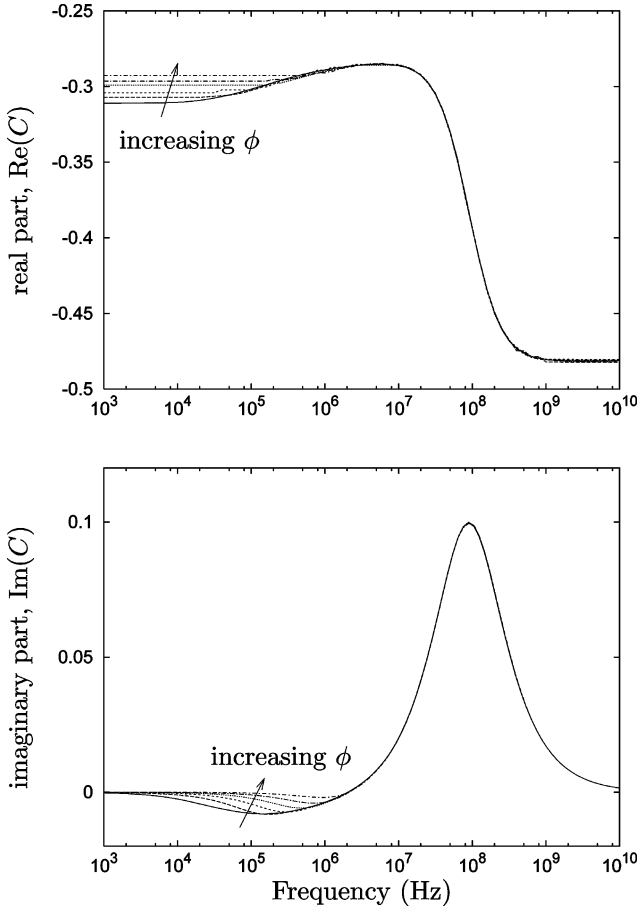

Figure 14. As in Figure 13 ($\kappa a = 50$) except $e\zeta/k_BT = 4$.

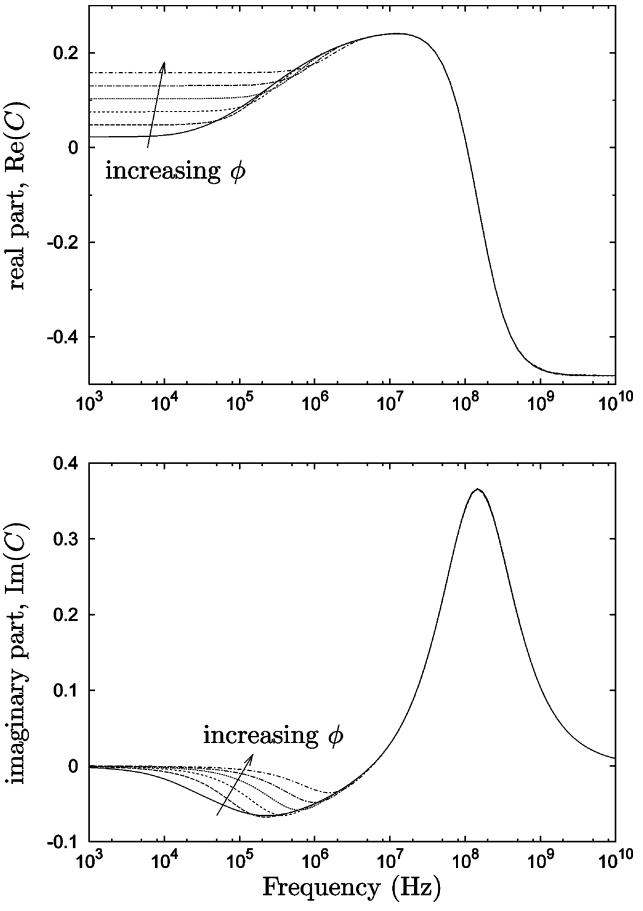

Figure 15. As in Figure 13 ($\kappa a = 50$) except $e\zeta/k_BT = 7$.

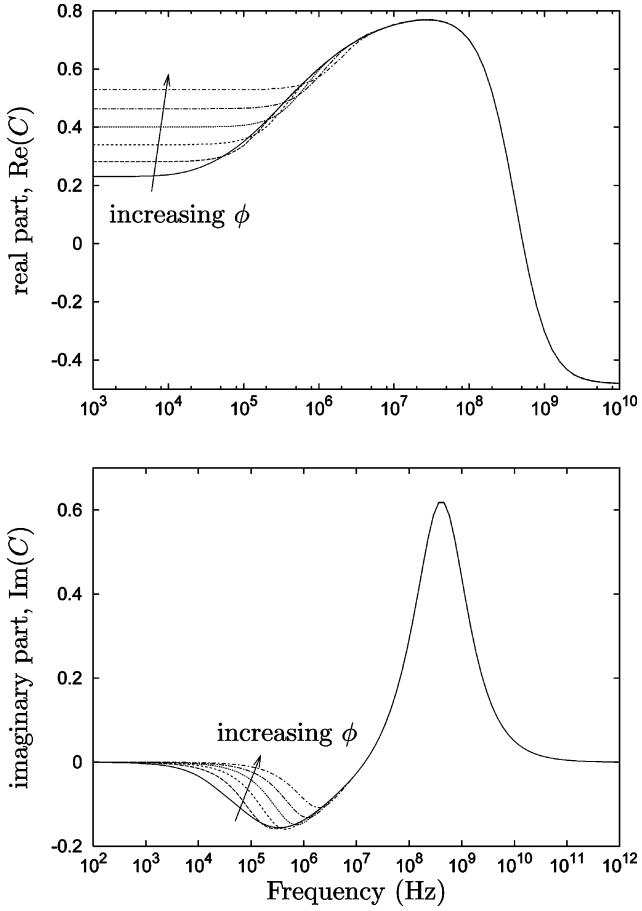

Figure 16. As in Figure 13 ($\kappa a = 50$) except $e\zeta/k_BT = 10$.

Of the real and imaginary parts of C, the imaginary part is least affected and then largely in a limited frequency regime centered around 10^5 Hz. Little variation fortuitously occurs at low frequencies where the imaginary part essentially vanishes, while at very high frequencies ion transport itself is not occurring as double layer ions cannot keep up with the field variation. On the other hand, the real part of C is predominantly affected in the low-frequency regime, which indicates that it is the static contribution to the dipole coefficient that is affected. As previously postulated,[28] the coefficient tends to the limiting value of $\sim -1/2$ at high frequencies and low ζ. In fact, our results indicate that this is the case for a large range of ζ: the dipole coefficient is clearly independent of ϕ for frequencies above the megahertz range for a large range of ζ potentials and also electrolyte concentrations (although we do not show this here).

When double layers are thicker (say, at extremes such as $\kappa a = 1$), even small particle concentrations ($\phi \approx 10^{-2}$) influence the dipole coefficient, even at low ζ potentials (data not shown). The variation of C with ϕ again increases as ζ increases. In this case both real and imaginary parts are significantly dependent on volume fraction.

We should mention that in contrast to the definition used by Mangelsdorf and White, i.e., C_{approx} in our terminology, our coefficient, C, is not linearly related to the conductivity increment (except at very low volume fractions). Consequently, the ϕ-dependence of C, when it appears, is not necessarily reproduced by ΔK^*, or vice versa. Moreover, when it does exhibit ϕ dependent behavior there is no immediate or intuitive way to predict how the coefficient will respond to volume fraction changes.

(28) Arroyo, F. J.; Carrique, F.; Ahualli, S.; Delgado, A. *V. Phys. Chem. Chem. Phys.* **2004**, *6*, 1446.

VI. Summary and Concluding Remarks

In this paper we have presented a full cell model of dynamic mobility and conductivity response of a finite volume suspension of charged particles to an external applied oscillating electric field. The equations are based on the fully self-consistent cell model (corrected) presented in an earlier paper,[1] but extended to include the calculation of the system's dielectric response. The numerical results given here focus on the complex conductivity increment and the Maxwell−Wagner coefficient, both of which are relevant to experimental works.

The cell model can be applied to systems with a large range of electrical double layer parameters and across a broad frequency spectrum. It remains robust at low volume fractions (very dilute systems), low frequency (the static case), and high-frequency limits. Moreover, it can also accommodate high ζ potentials and high salt concentrations. Our model reproduces previous analytic, asymptotic, and numerical results in many of these limiting cases. This suggests that the cell model approach has the potential to be a versatile alternative to the various approximate theories presented in the past.

In a follow-up paper, we will compare the model calculations with experimental data for a large set of system parameters.

[a]Note: One boundary condition was incorrect; however, the results displayed in ref 1 are only slightly altered. See Section II for details.

LA703777G